Pergamon

Int. Comm. Heat Mass Transfer, Vol. 30, No. 7, pp. 987-996, 2003

0735–1933/03/$–see front matter

Available online at www.sciencedirect.com

SCIENCE DIRECT®

PII: S0735-1933(03)00157-X

THERMAL CONTACT RESISTANCE CORRELATION FOR METALS ACROSS BOLTED JOINTS

C.L. Yeh and C.T. Lin
Da-Yeh University
Department of Mechanical and Automation Engineering
Changhua 51505
Taiwan, R.O.C.

(Communicated by J.P. Hartnett and W.J. Minkowycz)

ABSTRACT

An experimental study of thermal contact resistance was conducted with metallic contacts across bolted joints. Three types of interfaces were considered, including Al/Al, Cu/Al, and SS/Al contacts. The contact pressure of bolted interfaces was measured by the pressure-measuring film through an image processing technique. Results indicate that the contact pressure increases with the torque applied on bolts. The contact pressure also increases with either an increase in the number of bolts, or a decrease in the surface roughness of contacting surfaces. The thermal contact resistance of bolted junctions depends strongly on the interfacial contact pressure. Correlation of interfacial pressure was developed in terms of the torque and bolt-joined parameters. Contact resistance correlation was expressed as a function of the contact pressure, surface roughness, and material properties. Both correlations were in reasonable agreement with the experimental data obtained in this study.

Introduction

The importance of the thermal contact resistance in many engineering systems is well recognized. In the last decades, a great effort has been made in the theoretical prediction and the experimental measurement of the thermal contact resistance of metallic interfaces under a variety of conditions. Due to the differences in material properties, geometric configurations, mounting patterns, junction characteristics, and interstitial media, the scope of thermal contact

resistance is broad and complex. There have been several comprehensive reviews [1-5] summarizing the extensive topics in the field of contact resistance. Unfortunately, there is no satisfactory theory that will predict contact resistance for all types of the engineering materials, nor have experimental studies yielded completely reliable empirical correlations. This is understandable because various contacting conditions may be encountered in practice.

The theory developed by Cooper *et al.* [6] led to two dimensionless groups in the relation,

$$\frac{h_c}{k}\frac{\sigma}{\tan\theta} = 1.45\left(\frac{P}{H}\right)^{0.985} \tag{1}$$

where h_c is the thermal contact conductance, σ is the rms surface roughness, k is the thermal conductivity, $\tan\theta$ is the mean of absolute slope, P is the pressure, and H is the microhardness. Fletcher and Gyorog [7] in their correlation for similar metals in contact considered the following additional factors: (1) the mean junction temperature, (2) the coefficient of thermal expansion, and (2) a surface parameter accounting for the roughness as well as the flatness deviation of both surfaces. They also made use of the Young's modulus (E), rather than the microhardness, to nondimensionalize the pressure. The dimensional analysis of Thomas and Probert [8] yielded a dimensionless conductance $C^*=C/\sigma k$ and a dimensionless load $W^*=W/\sigma^2 H$. Their analysis showed C^* to be proportional to about $W^{*\,0.73}$ for aluminum and stainless steel contacts in vacuum. For a variety of metal powders or assemblies of metal fibers, Miller and Fletcher [9] developed a correlation formulated in terms of the physical properties of the porous material. The dimensionless expression is of the form

$$\frac{h_c t}{k} = 2.335\ \left[\frac{P}{H}(1-\varepsilon)\right]^{0.72} \tag{2}$$

where t is the sample thickness and ε is the porosity of the material. An equation was proposed by Al-Astrabadi et al. [10] to correlate the thermal contact conductance for stacks of thin metallic layers in vacuum. The correlation was similar to that of Eq. (2) by setting the porosity term equal to zero, and the pressure term exponent in the expression was found to be 0.58. Recently, a correlation describing the thermal contact resistance (R_c) of aluminum honeycombs in contact with metal blocks and the interfacial contact pressure (P_c) was developed by Yeh *et al.* [11] in the following form

$$\frac{R_c k_m}{\sigma} = 1.5\times 10^7 \left(\frac{P_c}{E'\varepsilon'}\right)^{-0.47} \tag{3}$$

where k_m is the harmonic mean thermal conductivity of two contacting materials, E' is a function of the modulus of elasticity (E) and Poisson's ratio (ν) associated with two contacting materials, and ε' is a function of the cell size of the honeycomb, the number of cells, and the apparent contact area.

This study represents an experimental investigation of the thermal contact resistance for metals across bolted joints. The contact pressure of the bolted interface was measured by pressure-measuring films. In particular, efforts were made towards the development of two empirical correlations. One formulated the interfacial contact pressure in terms of the sample dimension and bolt-joined parameters, such as torque, the number of bolts, and bolt size. The other correlated the thermal contact resistance as a function of the contact pressure, characteristic parameters of sample surfaces, and material properties.

Methods of Approach

Experimental Setup

A detailed description of the experimental setup, consisting of a guard heater, a main heater, a specimen insulation jacket, and a heat sink, has been previously reported [12]. The thermal contact resistance (R_c) is equal to the reciprocal of the thermal contact conductance (h_c), which is defined as the ratio of the mean heat flux (q) across the junction to the interfacial temperature difference (ΔT). The approach used to measure the heat flux and temperature difference across the bolted interface was given in Ref. 12. The interfacial contact pressure across the bolted junction was determined by the pressure-measuring film (Fuji Prescale Film). With a Prescale film inserted in the interface of bolted metals, once the torque is applied on the bolts, the exerted pressure results in a color development on the film. The color concentration on the pressed film is a function of the pressure. The calibration and image analysis procedures developed to convert the color concentration into the pressure were previously described [12].

Test Samples

Test specimens used in this study were metal blocks, with a square cross section and a height (H) of 50 mm. Three types of metals, including aluminum alloy 6061-T6 (Al), copper (Cu), and stainless steel 304 (SS), were adopted and their material properties are listed in Table 1.

The surface roughness and asperity slope of contacting surfaces were measured by a surface analyzer (Ommelwerke GMBH-T500). The test sample was composed of two metal blocks joined by bolts in various patterns. The surface parameters and bolt-joined configurations, including the number of bolt (N) and bolt size (D), of six pairs of test samples are summarized in Table 2. Figure 1 illustrates the position of bolts on the samples used in this study.

TABLE 1
Material Properties of Test Specimens

Material	Thermal Conductivity k, W/m-K	Modulus of Elasticity E, GPa	Poisson's Ratio ν
Aluminum 6061-T6	167	69	0.33
Copper (UNS C11000)	388	130	0.33
Stainless Steel 304	16.2	200	0.29

TABLE 2
Surface Parameters and Bolt-Joined Configurations of Test Specimens

Sample No.	Specimen Materials	Surface Roughness σ, μm	Absolute Asperity Slope $\tan\theta$	Cross-Sectional Area, A mm x mm	Number of Bolts (N)/ Bolt Size (D, mm)
1	Al/Al	0.10/0.11	0.04/0.04	63.5×63.5	4/8
2	Al/Al	0.84/0.70	0.14/0.12	63.5×63.5	4/8
3	Al/Al	0.14/0.19	0.05/0.06	63.5×63.5	8/8
4	Al/Al	0.90/0.87	0.15/0.14	63.5×63.5	8/8
5	Cu/Al	0.92/0.85	0.16/0.13	50.8×50.8	4/5
6	SS/Al	0.93/0.85	0.17/0.13	50.8×50.8	4/5

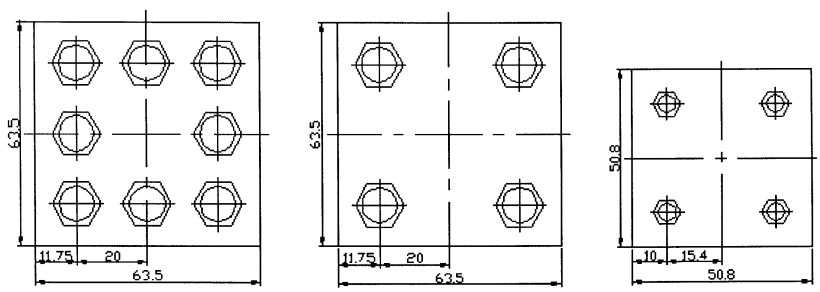

FIG. 1
Positions of bolts for test samples: (a) #3 and #4, (b) #1 and #2, and (c) #5 and #6 (unit: mm).

Results and Discussion

Interfacial Contact Pressure

Figure 2 shows a typical set of pressed Prescale films for the Sample #3 under different magnitudes of applied torque (τ). As can be seen in Fig. 2, the developed color concentration increases with the torque, implying an increase in the interfacial contact pressure. Figure 3 shows the variation average contact pressure (P_c) with the applied torque for different test samples. As expected, the contact pressure in bolted interfaces increases with the torque. Compared Samples #2 with #4, it is found that the contact pressure substantially increases when the number of bolts is twofold. Similar result was observed between Samples #1 and #3. Due to a smaller surface roughness, which represents a better contact, the contact pressure of Sample #1 is higher than that of Sample #2. The effect of surface roughness on contact pressures was also seen between Samples #3 and #4. In addition, it should be useful to note that even though Samples #5 and #6 was joined by four 5-mm bolts, they yielded larger contact pressures because of their smaller contact areas.

Based upon the experimental measurement, it was found that the contact pressure of bolt-joined interfaces was a function of the applied torque (τ), the number of bolts (N), the bolt size (D), the surface roughness of metals (σ), and the area in contact (A). The dimensional analysis yielded two dimensionless numbers, namely

$$P^* = \frac{P_c}{E'} \quad \text{and} \quad \tau^* = \frac{\pi ND}{S_y AH\sigma_c} \tag{4}$$

The parameter E' in the dimensionless pressure P^* is a function of the modulus of elasticity (E) and Poisson's ratio (ν) associated with two contacting materials and is expressed as [13]

$$\frac{1}{E'} = \frac{1-\nu_1^2}{E_1} + \frac{1-\nu_2^2}{E_2} \tag{5}$$

Parameters S_y and σ_c in the dimensionless torque τ^* are the yield strength of the bolt and the combined rms surface roughness of two contacting surfaces, respectively. The σ_c is defined as $\sigma_c = \sqrt{\sigma_1^2 + \sigma_2^2}$. Based upon all of the measured data, the correlation depicted in Fig. 4 between P^* and τ^* was obtained as

$$\frac{P_c}{E'} = 2.53\times10^{-3}\left(\frac{\pi ND}{S_y AH\sigma_c}\right)^{0.36} \tag{6}$$

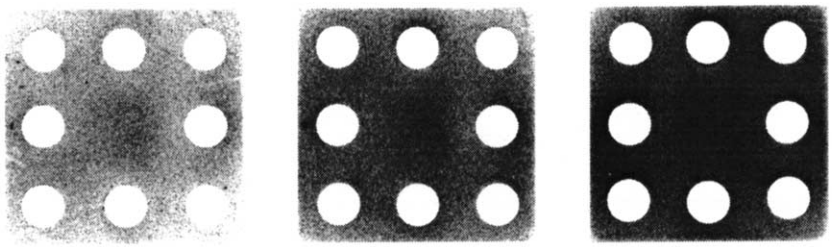

(a) $\tau = 2$ N-m (b) $\tau = 4$ N-m (c) $\tau = 6$ N-m

FIG. 2
Typical pressure-measuring films showing an increase in color concentration with increasing torque: (a) $\tau = 2$ N-m, (b) $\tau = 4$ N-m, and (c) $\tau = 6$ N-m.

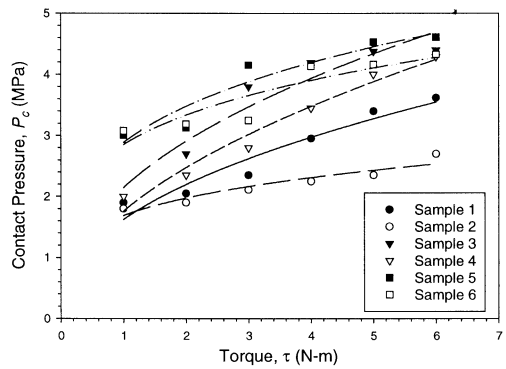

FIG. 3
Measured average contact pressures across bolted interfaces under different applied torques.

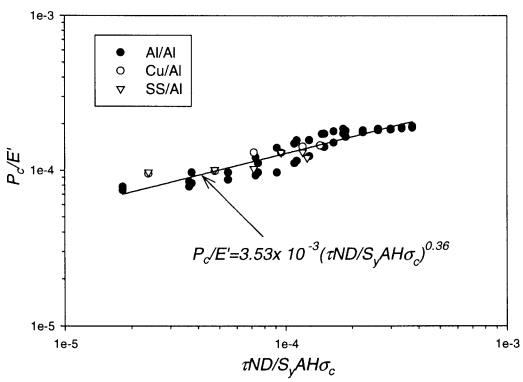

FIG. 4
Variation of dimensionless pressure with dimensionless torque for metal contacts joined by bolts.

As shown in Fig. 4, the correlation line is in good agreement with all of the measured data, indicating that the selection of dimensionless numbers, P^* and τ^*, is appropriate for this study.

Thermal Contact Resistance

Figure 5 shows the effect of applied torque on the measured thermal contact conductance (h_c) of three pairs of Al/Al samples. As shown in Fig. 5, the contact conductance increases obviously with the applied torque. This correspondingly suggests that the contact conductance increases with the increase of interfacial contact pressure. The effect of the number of bolts on the contact conductance can be observed by comparing Sample #3 (N = 8) and Sample #1 (N = 4) in Fig. 5. Moreover, the effect of the number of bolts on conductance appears to be more pronounced at larger torques. This can be explained by the fact that the difference in contact pressures becomes greater at larger torques, as shown in Fig. 3. In addition, due to a smaller surface roughness for Sample #3, the contact conductance of Sample #3 was higher than that of Sample #4. This was attributed to the smaller surface roughness the higher contact pressure. A smaller surface roughness also means more contact spots in the interface for heat transfer. Similarly, the discrepancy of contact conductance between Samples #3 and #4 caused by the surface roughness is more noticeable as the torque is increased.

Figure 6 shows the contact conductance of samples with Cu/Al (Sample #5) and SS/Al (Sample #6) contacts. It is evident that the contact conductance of Sample #5 is higher than that of Sample #6, since the thermal conductivity (k) of copper is significantly higher than that of stainless steel. It is also useful to note that the contact conductance of the SS/Al sample is nearly independent of the torque in the range of 1-5 N-m. This is because the modulus of elasticity (E) of stainless steel is large when compared with Al and Cu; thereby, the deformation of high spots on the contact surface is less, resulting in nearly no increase in the contact area for heat transfer with the torque.

According to the above observations, the thermal contact resistance (i.e., the reciprocal of the thermal contact conductance) is a function of the interfacial contact pressure (P_c), the surface roughness (σ), and the modulus of elasticity (E) and the thermal conductivity (k) of materials. The dimensional analysis led to two dimensionless groups, namely

$$R^* = \frac{R_c k_m}{(\sigma_c / \tan\theta_c)} \quad \text{and} \quad P^* = \frac{P_c}{E'} \tag{7}$$

The parameter k_m in the dimensionless resistance R^* is harmonic mean thermal conductivity of two contacting metals and is expressed as [14]

$$k_m = \frac{2k_1k_2}{(k_1 + k_2)} \tag{8}$$

The parameter $\tan\theta_c$ in R^* represents a combined absolute asperity slope and is defined as $\tan\theta_c = \sqrt{\tan\theta_1^2 + \tan\theta_2^2}$. The resulting correlation between R^* and P^* is expressed as

$$\frac{R_c k_m}{(\sigma_c / \tan\theta_c)} = 1.08\times10^{-8}\left(\frac{P_c}{E'}\right)^{-3.0} \tag{9}$$

The contact resistance correlation in comparison with all of the measured data is shown in Fig. 7. Some scatter was to be expected because of possible uncertainties in the measured heat flux, temperature different, and interfacial contact pressure. Based upon the uncertainty analysis [12], the overall uncertainty in this study was about 7.3%.

Conclusions

This study provides experimental data of thermal contact resistance in the Al/Al, Cu/Al, and SS/Al bolted interfaces. In addition, the interfacial contact pressure was measured by the pressure-measuring film, which allowed the visualization of pressure distribution. The contact

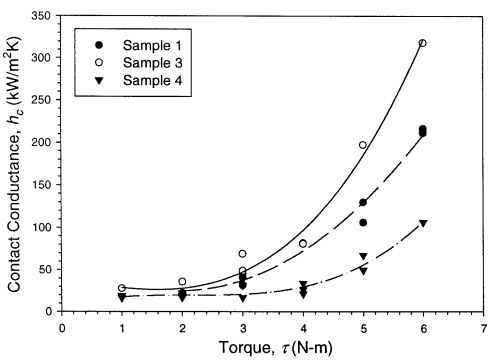

FIG. 5
Effect of torque on thermal contact conductance of Al/Al bolted interfaces.

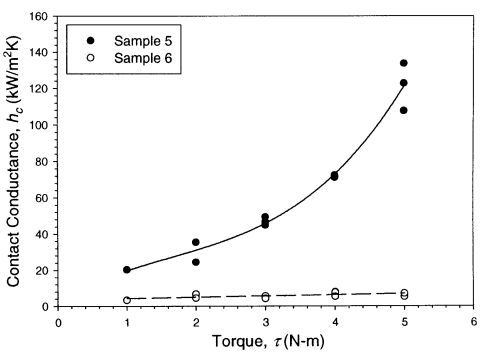

FIG. 6
Effect of torque on thermal contact conductance of Cu/Al and SS/Al bolted interfaces.

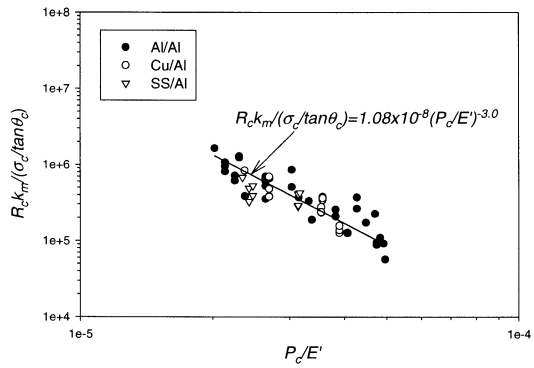

FIG. 7
Variation of dimensionless contact resistance with dimensionless pressure for metal contacts joined by bolts.

pressure increases with the torque applied on bolts. Effects of the bolted-joined pattern and the surface roughness of samples on the contact pressure are important, as well. The increase of the number of bolts from 4 to 8 leads to a significant increase in contact pressure. The thermal contact resistances of Al/Al and Cu/Al interfaces depend strongly on the contact pressure. The relatively low contact conductance for SS/Al contacts was mainly caused by the low thermal conductivity of stainless steel. Due to the high modulus of elasticity of stainless steel, the increase of contact pressure yields nearly no effect on the contact conductance of SS/Al samples. Two empirical correlations were successfully developed for the interfacial contact pressure and contact resistance of bolted metallic joints. Compared with the experimental data obtained in this investigation, it is suggested that the correlation equations can be used to accurately predict the interfacial pressure and contact resistance for bolted metallic junctions.

References

1. C.V. Madhusudana and L.S. Fletcher, *AIAA J.* 24, 510 (1986).
2. L.S. Fletcher, *ASME J. Heat Transfer* 110, 1059 (1988).
3. M.A. Lambert and L.S. Fletcher, *J. Thermophysics Heat Transfer* 7, 547 (1993).

4. B. Snaith, S.D. Probert, and P.W. O'Callaghan, *Applied Energy* 22, 31 (1986).

5. M.R. Sridhar and M.M. Yovanovich, *J. Thermophysics Heat Transfer* 8, 633 (1994).

6. M.G. Cooper, B.B. Mikic, and M.M. Yovanovich, *Int. J. Heat Mass Transfer* 12, 279 (1969).

7. L.S. Fletcher and D.A. Gyorog, Heat Transfer and Spacecraft Thermal Control, in *Progress in Astronautics and Aeronautics*, vol. 24, MIT Press, Cambridge, Mass., pp. 273-288 (1971).

8. R. Thomas and S.D. Probert, *ASME J. Heat Transfer* 94, 276 (1972).

9. R.G. Miller and L.S. Fletcher, Heat Transfer with Thermal Control Applications, in *Progress in Astronautics and Aeronautics*, vol. 39, MIT Press, Cambridge, Mass., pp. 81-92 (1975).

10. F.R. Al-Astrabadi, P.W. O'Callaghan, S.D. Probert, and A.M. Jones, *ASME J. Heat Transfer* 99, 139 (1977).

11. C.L. Yeh, Y.F. Chen, C.Y. Wen, and K.T. Li, *Exp. Heat Transfer*, in press (2003).

12. C.L. Yeh, C.Y. Wen, Y.F. Chen, S.H. Yeh, and C.H. Wu, *Exp. Thermal Fluid Sci.* 25, 349 (2001).

13. B.B. Mikic, *Int. J. Heat Mass Transfer* 17, 205 (1974).

14. G.P. Peterson and L.S. Fletcher, *ASME J. Heat Transfer* 110, 996 (1988).

Received March 24, 2003